Turbulence Modeling in Stratified Flows over Topography

Sutanu Sarkar
University of California at San Diego
La Jolla, CA 92093
Tel: 858-534-824, Fax: 858-534-7599, sarkar@ucsd.edu

Award N00014-05-1-0334
http://maeweb.ucsd.edu/fluids.html#SARKAR

LONG-TERM GOALS

The goal is to assess the ability of LES with modern subgrid turbulence closures to predict and understand transport and mixing in stratified flows over boundaries.

OBJECTIVES

- perform large eddy simulation (LES) of canonical turbulent flows over boundaries and compare against available laboratory, field and direct numerical simulation (DNS) data using metrics of mean flow profiles, Reynolds stresses and dissipation rate.
- quantify the effect of grid resolution, Reynolds number and stratification level on model performance.
- represent oceanic small-scale mixing processes in the AESOP experiment using fine-resolution LES and help understand field data.

APPROACH

A non-hydrostatic code that numerically solves the unsteady, three-dimensional, primitive equations is used. Advanced models such as the dynamic mixed model and the dynamic eddy viscosity model are utilized to represent subgrid processes in the LES approach. A novel near-wall model has been developed so as to increase the Reynolds number of boundary flows to realistically large geophysical values. The code is capable of capturing the effect of bottom slopes, small-scale roughness, and oscillatory forcing.

WORK COMPLETED

Near wall model

When simulating geophysical boundary layers at a large Reynolds number, in addition to the subgrid model for the outer layer, a near-wall model (NWM) is inevitable for handling the inner layer. This is due to the fact that the filter scale is typically much larger than the viscous/roughness scales, the generation of turbulence at the rough wall is not resolved, and consequently the near-wall Reynolds shear stress must be explicitly accounted for through a model. This issue has ben faced by the atmospheric boundary layer (ABL) community, where it is known that LES overpredicts the mean shear near the surface [7, 5] relative to expected similarity theory. Procedures to circumvent the problem with a near-wall mocenteringdel have been advanced [7, 11, 10], but there is no well-accepted solution.

Report Documentation Page

Form Approved
OMB No. 0704-0188

1. REPORT DATE	2. REPORT TYPE	3. DATES COVERED
30 SEP 2007	**Annual**	**00-00-2007 to 00-00-2007**

4. TITLE AND SUBTITLE	5a. CONTRACT NUMBER
Turbulence Modeling In Stratified Flows Over Topography	5b. GRANT NUMBER
	5c. PROGRAM ELEMENT NUMBER
6. AUTHOR(S)	5d. PROJECT NUMBER
	5e. TASK NUMBER
	5f. WORK UNIT NUMBER
7. PERFORMING ORGANIZATION NAME(S) AND ADDRESS(ES) **University of California at SanDiego,LaJolla,CA,92093**	8. PERFORMING ORGANIZATION REPORT NUMBER
9. SPONSORING/MONITORING AGENCY NAME(S) AND ADDRESS(ES)	10. SPONSOR/MONITOR'S ACRONYM(S)
	11. SPONSOR/MONITOR'S REPORT NUMBER(S)

12. DISTRIBUTION/AVAILABILITY STATEMENT
Approved for public release; distribution unlimited

13. SUPPLEMENTARY NOTES
code 1 only

14. ABSTRACT

15. SUBJECT TERMS

16. SECURITY CLASSIFICATION OF:			17. LIMITATION OF ABSTRACT	18. NUMBER OF PAGES	19a. NAME OF RESPONSIBLE PERSON
a. REPORT	b. ABSTRACT	c. THIS PAGE			
unclassified	**unclassified**	**unclassified**	**Same as Report (SAR)**	**10**	

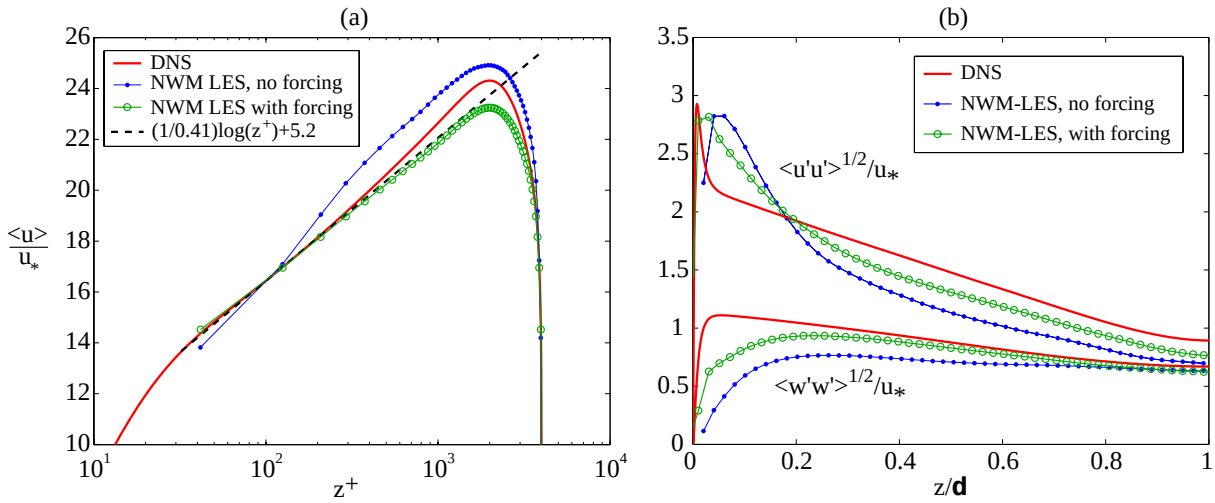

Figure 1: (a) Mean velocity profiles and (b) streamwise and wall-normal r.m.s velocity for smooth wall channel flow with $Re_* = 2000$. The performance of the near-wall model (NWM) is assessed by comparison with DNS data.

Near-wall models for geophysical boundary layers are commonly formulated by applying an approximate boundary condition at the wall, an unsteady generalization of the log law. That proposed by Marusic *et al.* [6] which will be referred to here as the MKP model has been adopted. The MKP model is formulated as the following approximate wall boundary condition:

$$\frac{\tau_{w,i}(x,y,t)}{\rho_0 u_*^2} = \frac{U_i(1)}{(U(1)^2+V(1)^2)^{1/2}} - \beta\frac{[u_i(x+\Delta_s,y,z(1)) - U_i(1)]}{u_*}, \tag{1}$$

where $z(1)$ is the location of the gridpoint nearest the wall and U(1) and V(1) are the plane averaged horizontal velocity components at the first gridpoint. Marusic *et al.* [6] hypothesized that the constant β should be universal, and empirically determined $\beta \simeq 0.10$. The instantaneous friction velocity and mean wall stress are estimated by assuming that the plane-averaged velocity at the first gridpoint follows the expected log law. Note that the friction velocity, u_*, and surface stress angle, α, do not have to be prescribed *a priori* but are a product of the simulation.

The MKP near-wall model along with the dynamic eddy viscosity model in the exterior has been tested by us for smooth and rough channel flow, and for a bottom Ekman layer with and without stratification. In *all* cases, the mean velocity is *overpredicted* with respect to the log law. This trend is illustrated with channel flow at the friction Reynolds number, $Re_* = 2000$, where the direct numerical simulation (DNS) of Hoyas and Jimenez [4] is available for comparison. Figure (a) shows the mean velocity profiles as a function of $z^+ = zu_*/\nu$ for smooth wall channel flow simulations. The mean velocity from the DNS follows the expected log law between $z^+ > 30$ and $z/\delta < 0.2$. It is apparent from Figure (a) that the NWM-LES without stochastic forcing (blue line with filled circles) overpredicts the mean shear where a log law is expected. A novel solution based on adaptive stochastic forcing has been developed as described in detail and validated by Taylor and Sarkar [15]. A summary is given below.

Adaptive stochastic forcing

A stochastic forcing term is added to the r.h.s of the wall normal momentum equation so as to enhance the vertical velocity fluctuations while modifying the local Reynolds stress according to the expected value from the log law. The characteristic length and time scales of the forcing are set by the grid-size and time-step, respectively. The proposed forcing function can be written

$$f_z(x,y,z) = \pm\mathcal{R}A(z), \tag{2}$$

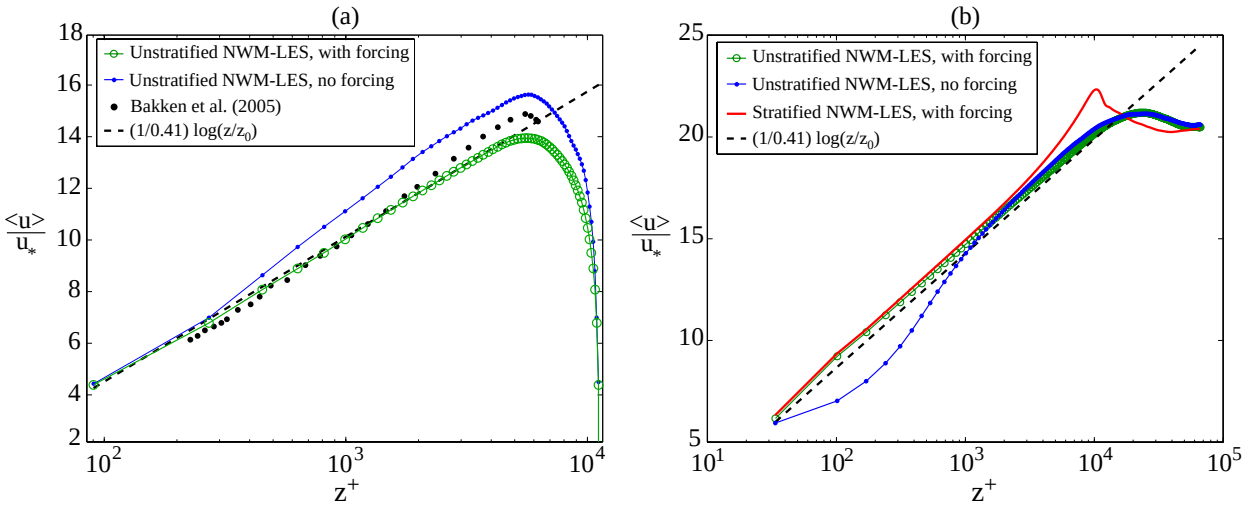

Figure 2: (a) Mean velocity profiles for rough wall channel flow with $z_0/\delta = 2.81x10^{-3}$ ***and*** $Re_* = 5600$***, (b) Mean velocity profiles for a bottom Ekman layer with*** $z_0/\delta = 5.7 * 10^{-5}$ ***and*** $Re_* = 60,00$***.***

where $\mathcal{R}$ is a random number between 0 and 1 and $A(z)$ is an amplitude function. The forcing amplitude is evaluated dynamically in order to ensure that the mean velocity follows the logarithmic law near the wall. The difference between the resolved shear and the expected logarithmic law value is

$$e(z) = \frac{\kappa z}{u_*}\left(\frac{d\langle u\rangle}{dz}^2 + \frac{d\langle v\rangle}{dz}^2\right)^{1/2} - 1. \tag{3}$$

The forcing amplitude can then be locally adjusted using a proportional controller with

$$A(z)^{n+1} = A(z)^n + \frac{u_* e(z)}{\tau}, \tag{4}$$

where τ sets the relaxation time and should be large enough to allow the flow to adjust to the forcing, and typically we have used $\tau \approx \delta/u_*$. The sign of the r.h.s of Eq. (2) is chosen to increase or decrease the u', w' correlation according to the sign of $e(z)$. The stochastic forcing must satisfy the following constraints: its amplitude must be small and its width in physical space be thin so that the "large eddies" external to the near-wall region are not artificially forced. These constraints are met, for example, in the rough Ekman layer, the amplitude is less than 6% of the r.m.s vertical velocity and is non-zero only for 5 points near the boundary, less than 8% of the boundary layer thickness.

Returning to the example in Fig. (a), it can be seen that a much better agreement with the DNS in the logarithmic region is achieved when the stochastic forcing term is included. The streamwise and wall-normal turbulent velocities are shown in Figure (b). When the NWM-LES is used, the magnitude of the wall-normal *rms* velocity is significantly less than the DNS. Adding stochastic forcing increases the wall-normal velocity fluctuations as expected, and results in a better agreement with the DNS. The same conclusion is true for the spanwise velocity fluctuations (not shown for clarity). Without forcing, the streamwise velocity fluctuations compare reasonably well in magnitude to the DNS, but an improvement is still seen when forcing is added, resulting in a shift in the location of the maximum near the wall and an increase in the outer layer fluctuations. Fig. (a) shows the example of a rough boundary layer where a comparison is made with experiments of Bakken *et al.* [2] where wire mesh was used to roughen the ceiling and floor of a wind tunnel. The friction Reynolds number is 5600, and the roughness length scale is $k^+ = 187$

Table 1: Physical Parameters

Ri_*	N_∞/f	Re_*	Pr	u_*/U_∞	z_0/δ	α_0
0	0	$1.08 * 10^6$		0.0488	$4.80 * 10^{-5}$	15.4^o
1000	31.6	$1.09 * 10^6$	***5-10***	0.0490	$4.78 * 10^{-5}$	18.9^o
5625	75	$1.12 * 10^6$		0.0497	$4.71 * 10^{-5}$	24.8^o

indicating that the flow is fully rough. Fig. (b) shows an application to an unstratified bottom Ekman layer where a rough-wall log-law is expected to hold throughout. In both examples, the results with forcing (green line with unfilled circles) are much better than without (blue line with filled circles).

Bottom Ekman layer under a current

A stratified bottom Ekman layer over a non-sloping, rough surface has been studied using large-eddy simulation in order to examine the effects of the outer layer stratification on the boundary layer structure. Three-dimensional, unsteady simulations of a stratified bottom Ekman layer have not been performed before although the ABL analog of a boundary layer stratified through a surface cooling heat flux has been. Details of our LES investigation are given by Taylor and Sarkar [14]; a summary follows below.

The turbulent Ekman layer considered here is formed when a steady flow in geostrophic balance encounters a flat boundary. The x-axis is aligned with the external, steady zonal flow in geostrophic balance. The seafloor is represented by a non-sloping, rough surface. The roughness elements are too small to resolve directly by the grid, but their effect is parameterized through a near-wall model. The seafloor is also assumed to be adiabatic. The boundary conditions are periodic in the horizontal directions; a sponge layer along with a non-reflecting boundary condition is used in the vertical. The domain size is approximately $2\delta \times 2\delta \times 2\delta$ where $\delta = u_*/f \approx 100m$. The parameters considered in this study are listed in Table 1. Note that Re_∞ is the same for each simulation, but the drag coefficient depends on the outer layer stratification, and hence the friction Reynolds number varies between each case. We have performed simulations at three different values of Ri_*, equivalent to changing the free-stream density gradient. For comparison with oceanographic conditions, observations of the bottom boundary layer over the Oregon shelf by Perlin et al. [8, 9] provide estimates of $Re_* = 4 * 10^4 - 8 * 10^5$ and $N/f = 75$. Therefore, both the Reynolds numbers and stratification levels considered in the present study are comparable with field data. In order to compare our simulation results to realistic conditions, we will use $U_\infty = 0.2m/s$, $f = 10^{-4}s^-1$, and $\nu = 10^{-6}m^2/s$ which, assuming that $u_*/U_\infty = 0.05$, yields $\delta \approx 100m$ and $z_0 = 0.5cm$. The roughness lengthscale is consistent with observations by Perlin et al. [8] who found that $z_0 = 0.05$cm - 2 cm depending on the method used to infer the wall stress.

The subgrid scale stress tensor, $\boldsymbol{\tau}$, and the subgrid scale density flux, $\boldsymbol{\lambda}$, are evaluated using the dynamic Smagorinsky model [3]. The dynamic procedure avoids the empirical specification of the Smagoinsky coefficient and has been shown to perform well for wall-bounded flows and density stratified flows [1, 12]. Details of the basic LES model can be found in Armenio and Sarkar [1]. To avoid the need to resolve the very small turbulent motions near the lower wall, we have used the near-wall model (NWM) described previously in this report.

Mean properties of the boundary layer

The plane-averaged temperature profiles after the flow has reached quasi-steady state are shown in Figure 3(a). The components of the Reynolds averaged horizontal velocity are shown in Figure 3(b). Comparing with the temperature profiles, it is apparent that most of the Ekman transport is confined to the mixed layer. The increase in cross stream velocity results in a broadening of the

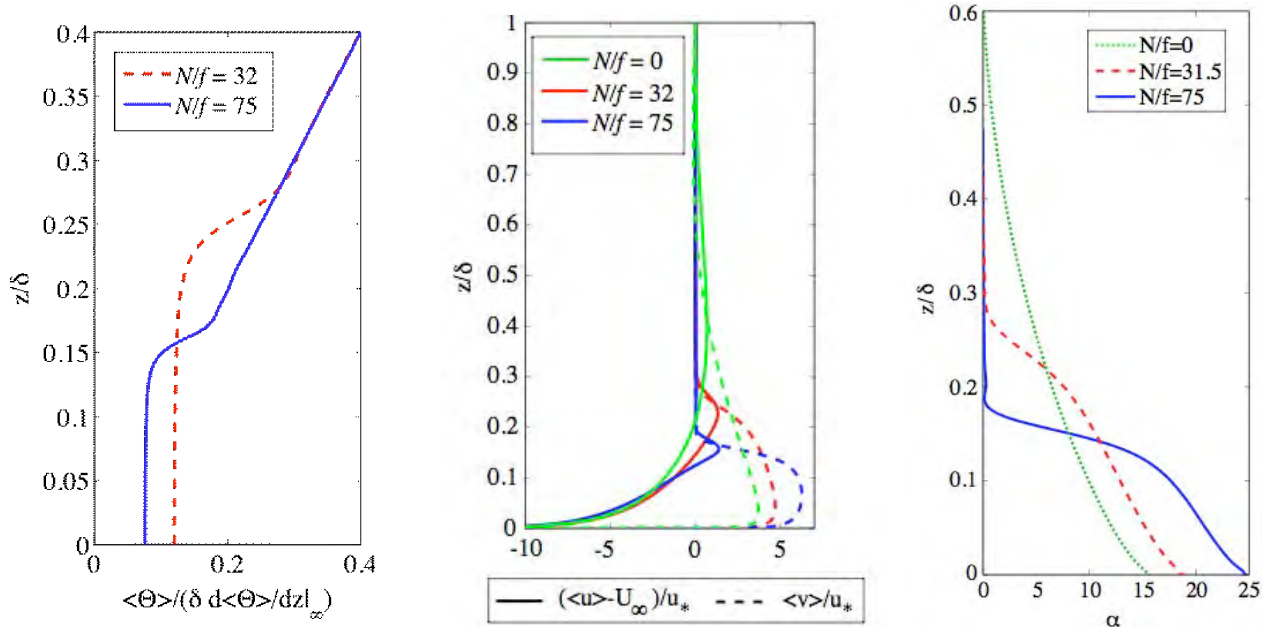

Figure 3: (a) Plane averaged temperature profiles, (b) Plane and time-averaged horizontal velocity components, (c) Angle of Ekman veering. Note that $\delta \approx 100\,m$ in this and the following figures.

Ekman spiral in a hogograph (not shown). It is interesting to note that while the density gradient is zero near the lower wall, the surface turning angle $\alpha_0 = tan^{-1}(\tau_y/\tau_x)$ increases with the outer layer stratification, as listed in Table 1. The angle of Ekman veering, defined by $\alpha = tan^{-1}\left(\frac{<v>}{<u>}\right)$ is shown as a function of z/δ in Figure 3(c). When the flow is unstratified, the turning of the mean velocity occurs gradually throughout the boundary layer. The rate of turning in the mixed layer does not depend strongly on the outer layer stratification. Therefore, since the magnitude of the turning angle at the wall increases with the outer layer stratification, and the boundary layer height decreases significantly, the rate of turning, $d\alpha/dz$, becomes very large in the pycnocline.

The mixed layer height decreases strongly with increasing N with a value of $15\,m$ at $N/f = 75$, Fig. 3(a). The boundary layer height based on the mean velocity also decreases strongly with increasing stratification as can be inferred from Fig. 3(b). Zilitinevich and co-workers have proposed a scaling law based on a combination of theory, field data [16] and simulations [17]:

$$h_{ZE} = C_R \frac{u_*}{f}\left(1 + \frac{C_R^2 C_{uN}}{C_S^2}\frac{N_\infty}{f}\right)^{-1/2}, \tag{5}$$

where the constants $C_R = 0.5$ and $C_{uN}/C_S^2 = 0.56$ were determined by fitting to data from large-eddy simulation. We define the boundary layer height as the location where the Reynolds stress $\left(\langle u'w'\rangle^2 + \langle v'w'\rangle^2\right)^{1/2} = 0.1u_*^2$. This estimate agrees well with the values given by the correlation, Eq. (5), namely, a boundary layer depth of $h/\delta = 0.215$ and $h/\delta = 0.147$ for $N/f = 31.6$ and $N/f = 75$.

The density gradient intensifies at the top of the mixed layer to form a bottom pycnocline, shown in Figure 4(a). The zonal velocity has the following interesting feature: a zonal jet with higher than the outer geostrophic velocity forms in the pycnocline, Figure 4(b). A peculiar feature of the mean velocity profile when $N/f = 75$ is that the mean velocity and the mean shear are maximum at the *same* location near the center of the pycnocline, Figure 4(c).

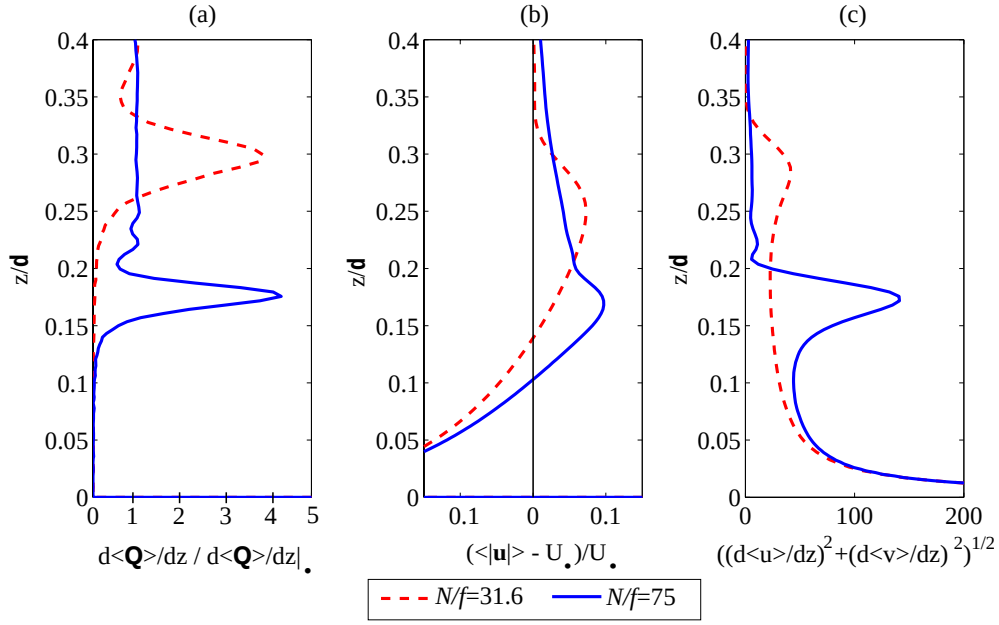

Figure 4: (a) Temperature gradient, (b) horizontal velocity magnitude (c) mean shear

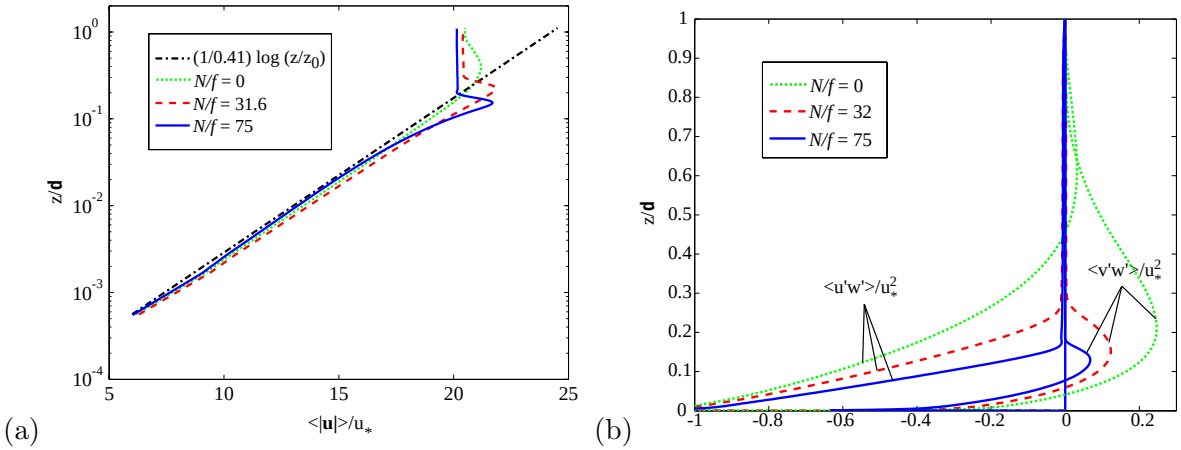

Figure 5: Reynolds averaged horizontal velocity magnitude

The law-of-the-wall is expected to hold in a region far enough from the wall where viscosity/roughness scale can be neglected, but near enough to the wall so that the boundary layer depth is not felt. The Reynolds averaged horizontal velocity magnitude on a semi-logarithmic scale is shown in Figure 5(a). Very near the wall, all cases are in reasonably good agreement with the unstratified logarithmic law. Deviations from the logarithmic velocity profile in the cases when stratification is present can be seen clearly by calculating the normalized velocity gradient,

$$\Phi = \frac{\kappa z}{u_*} \left| \frac{d < \mathbf{u} >}{dz} \right|. \tag{6}$$

The quantity Φ can be interpreted as the ratio of the observed mean velocity gradient to that expected from the logarithmic law. When the outer layer is stratified, the mean shear in the pycnocline increases significantly to $\Phi = 2$. It is worth noting that deviations from the law-of-the-wall begin well within the mixed layer.

Turbulence properties of the boundary layer

One consequence of the damping of turbulence by stratification is a decrease in the turbulent stresses, $< u'w' >$ and $< v'w' >$. The decrease in boundary layer height with increasing stratification is very apparent from the Reynolds stress profiles shown in Figure 5(b). Here, the Reynolds stress includes both the resolved and subgrid scale contributions. Note that above the boundary layer, the Reynolds stress approaches a small, nonzero value owing to the presence of turbulence-generated internal gravity waves. However, the Reynolds stress associated with the waves is much smaller than in the turbulent region, so this does not interfere with the definition of boundary layer height. It is evident from Figure 5(b) that the Reynolds stresses change more rapidly with height when the outer layer stratification is stronger. It can be shown that the behavior of the Reynolds stresses in the outer layer is consistent with the formation of the zonal jet observed in Fig. 4(b).

The plane-averaged turbulent kinetic energy budget can be found by dotting $\mathbf{u}'$ into the perturbation momentum equations:

$$\frac{1}{2}\frac{\partial < u_i' u_i' >}{\partial t} = -\frac{1}{2}\frac{\partial}{\partial z} < w' u_i' u_i' > -\frac{\partial}{\partial z} < w' p' > + \frac{1}{Re_\tau}\frac{\partial^2 k}{\partial z^2} - < S_{ij} >< u_i' u_j' > - \frac{1}{Re_\tau} < \frac{\partial u_i'}{\partial x_j}\frac{\partial u_i'}{\partial x_j} > - Ri_\tau < w'\rho' > - \frac{\partial}{\partial z} < u_i' \tau_{31} > + < \tau_{ji}\frac{\partial u_i'}{\partial x_j} > = \frac{\partial k}{\partial t} = 0. \tag{7}$$

Reading from left to right, the terms on the right hand side of Eq. (7) can be identified as the turbulent transport, pressure transport, viscous diffusion, production, dissipation, buoyancy flux, subgrid transport and subgrid dissipation, respectively. The leading terms in the turbulent kinetic energy budget for $N_\infty/f = 75$ is shown in Figure . Near the wall, the leading order balance is between production and dissipation and does not differ significantly from the unstratified case as shown in the inset. In the upper portion of the mixed layer, the turbulent transport appears as a source term representing the advection of turbulent eddies towards the pycnocline. Pressure transport, buoyancy flux, and dissipation represent the dominant energy sinks in the upper mixed layer. In the pycnocline, starting at about $z/\delta = 0.15$, the turbulent transport and buoyancy flux decrease as stratification suppresses the turbulent motion while pressure transport becomes the dominant source term. When the pressure transport is positive the vertical energy flux, $< p'w' >$ is increasing with height, consistent with an internal wave field that is gaining energy. This is direct evidence of the generation of internal waves by the interaction between boundary layer turbulence and a stable stratification, as examined in detail by us in a previous study [13].

IMPACT/APPLICATIONS

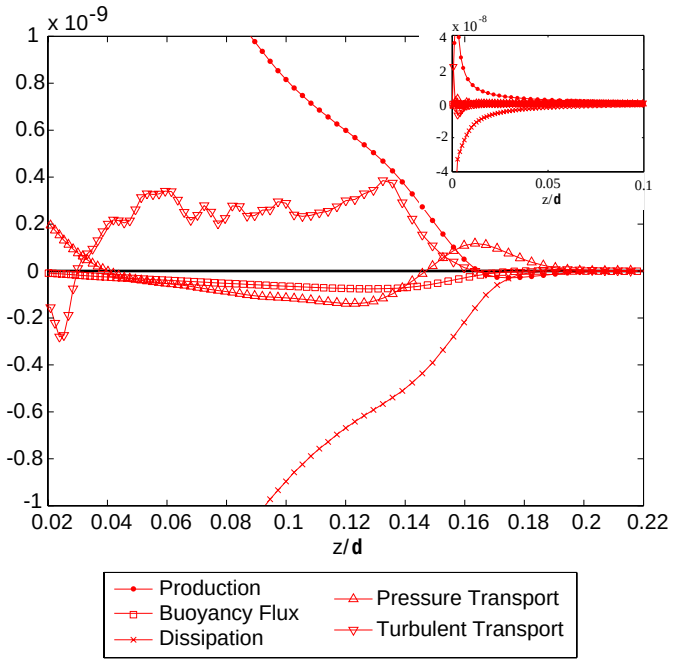

Figure 6: Turbulent kinetic energy budget at the top of the mixed layer and pycnocline for $N_\infty/f = 75$. Inset shows the TKE budget near the wall.

The detailed mean and turbulence structure of a stratified BBL has been obtained using LES. The height of the BBL and the drag coefficient are outputs and, thus, can be used as inputs for regional models. A new near-wall model with adaptive stochastic forcing has been developed to solve the problem of mean velocity over-prediction near the boundary in previous simulations.

References

[1] V. Armenio and S. Sarkar. An investigation of stably stratified turbulent channel flow using large-eddy simulation. *J. Fluid Mech.*, 459:1–42, 2002.

[2] O.M. Bakken, P. Krogstad, A. Ashrafian, and H.I. Andersson. Reynolds number effects in the outer layer of the turbulent flow in a channel with rough walls. *Phys. Fluids*, 17(165101):1–16, 2005.

[3] M. Germano, U. Piomelli, P. Moin, and W.H. Cabot. A dynamic subgrid-scale eddy viscosity model. *Phys. Fluids*, A3(7):1760–1765, 1991.

[4] S. Hoyas and J. Jimenez. Scaling of velocity fluctuations in turbulent channels up to $Re_\tau = 2000$. *Phys. Fluids*, 18:011702, 2006.

[5] S. Khanna and J. G. Brasseur. Analysis of Monin-Obukhov similarity from large-eddy simulation. *J. Fluid Mech.*, 345(6):251–286, 1997.

[6] I. Marusic, G.J. Kunkel, and F. Porte-Agel. Experimental study of wall boundary conditions for large-eddy simulations. *J. Fluid Mech.*, 446:306–320, 2001.

[7] P. J. Mason and D. J. Thomson. Stochastic backscatter in large-eddy simulations of boundary layers. *J. Fluid Mech.*, 242:51–78, 1992.

[8] A. Perlin, J.N. Moum, J.M. Klymak, M.D. Levine, T.J. Boyd, and P.M. Kosro. A modified law-of-the wall applied to oceanic bottom boundary layers. *J. Geophys. Res.*, 110:C10S10 (1–9), 2005.

[9] A. Perlin, J.N. Moum, J.M. Klymak, M.D. Levine, T.J. Boyd, and P.M. Kosro. Organization of stratification, turbulence, and veering in bottom Ekman layers. *J. Geophys. Res.*, in press, 2007.

[10] R. Stoll and F. Porte-Agel. A scale-dependent dynamic model for large-eddy simulations: application to a neutral atmospheric boundary layer. *J. Fluid Mech.*, 415:261–284, 2000.

[11] P. P. Sullivan, J. C. McWilliams, and C.-H. Moeng. A subgrid-scale model for large-eddy simulation of planetary boundary-layer flows. *Boundary-Layer Metl.*, 71:247–276, 1994.

[12] J. Taylor, S. Sarkar, and V. Armenio. An investigation of stably stratified turbulent channel flow using large-eddy simulation. *Phys. Fluids*, 17:116602(1–18), 2005.

[13] J. R. Taylor and S. Sarkar. Internal gravity waves generated by a turbulent bottom Ekman layer. *J. Fluid Mech.*, 590:331–354, 2007.

[14] J. R. Taylor and S. Sarkar. Stratification effects in a bottom Ekman layer. *J. Phys. Oceanogr.*, submitted, 2007.

[15] J.R. Taylor and S. Sarkar. Near-wall modeling for large-eddy simulation of an oceanic bottom boundary layer. *Proceedings of the Fifth Int. Symposium on Environmental Hydraulics*, 2007.

[16] S.S. Zilitinkevich and A. Baklanov. Calculation of the height of stable boundary layers in practical applications. *Boundary-Layer Meteorology*, 105(3):389–409, 2002.

[17] S.S. Zilitinkevich and I.N. Esau. On integral measures of the neutral barotropic planetary boundary layer. *Boundary-Layer Meteorology*, 104(3):371–379, 2002.